INTERNATIONAL JOURNAL FOR NUMERICAL METHODS IN FLUIDS
Int. J. Numer. Meth. Fluids 2018; **00**:1–23
Published online in Wiley Online Library (www.onlinelibrary.wiley.com). DOI: 10.1002/fld.4490

A new weighting method for improving the WENO-Z scheme

Shengping Liu[1,2],Yiqing Shen[1,2*], Fangjun Zeng[1,2], Ming Yu[3]

[1] *State Key Laboratory of High Temperature Gas Dynamics, Institute of Mechanics, Chinese Academy of Sciences, Beijing, China, 100190,*
[2] *School of Engineering Science, University of Chinese Academy of Sciences, Beijing, China, 100049,*
[3] *Institute of Applied Physics and Computational Mathematics, Beijing, China, 100094*

SUMMARY

The calculation of the weight of each sub-stencil is very important for a weighted essentially non-oscillatory (WENO) scheme to obtain high-order accuracy in smooth regions and keep the essentially non-oscillatory property near discontinuities. The weighting function introduced in the WENO-Z scheme provides a straightforward method to analyze the accuracy order in smooth regions. In this paper, we construct a new sixth-order global smoothness indicator (GSI-6) and a function about GSI-6 and the local smoothness indicators (IS_k) to calculate the weights. The analysis and numerical results show that, with the new weights, the scheme satisfies the sufficient condition for fifth-order convergence in smooth regions even at critical points. Meanwhile, it can also maintain low dissipation for discontinuous solutions due to relative large weights assigned to discontinuous sub-stencils. Copyright © 2018 John Wiley & Sons, Ltd.

Received …

KEY WORDS: WENO-Z scheme, global smoothness indicator, weighting function, low numerical dissipation

1. INTRODUCTION

The weighted essentially non-oscillatory (WENO) schemes have now become a kind of popular method in computational fluid dynamics[1]. The basic idea of WENO schemes is that: the numerical flux is calculated by using a convex combination of all the local numerical fluxes of candidate sub-stencils, each being assigned a nonlinear weight which determines the contribution of this sub-stencil. The weights can be designed as follows: in smooth regions, they approach certain optimal weights to achieve a high-order of accuracy, while in regions near discontinuities, the sub-stencils which contain the discontinuities are assigned small weights to keep the property of essentially non-oscillatory. Hence, an important issue for developing WENO schemes is how to evaluate the smoothness of sub-stencils and also weights.

In the first WENO scheme, Liu et al.[2] used a linear combination of the squares of all hierarchical undivided differences to measure the smoothness of a numerical flux on a sub-stencil. Later, the

*Correspondence to: State Key Laboratory of High Temperature Gas Dynamics, Institute of Mechanics, Chinese Academy of Sciences, No.15 Beisihuanxi Road, Beijing, China, 100190, E-mail: yqshen@imech.ac.cn

analysis of Jiang and Shu[3] showed that the WENO scheme constructed from a rth order ENO scheme[4] with the smoothness measurement of Liu et al. is only $(r+1)$th order accurate, and a classical way, which uses a sum of the L^2 norms of all the derivatives of the interpolation polynomial over the interval of integration, was proposed to calculate the local smoothness indicators (LSIs). Then, Balsara and Shu[5] extended the WENO scheme up to eleventh-order. In [6], Henrick et al. derived the necessary and sufficient conditions for fifth-order convergence of a fifth-order WENO scheme, and pointed out that the weights generated by the method of Jiang and Shu[3] cannot meet the conditions at critical point where the first derivative is zero. In their work [6], a mapping function for the weights is proposed, and the new mapped WENO (WENO-M) scheme can achieve fifth-order convergence in smooth regions including critical points.

In [7], Borges et al. proposed a different method to calculate weights by incorporating the higher-order information (global smoothness indicator, abbreviated to GSI) about the regularity of the numerical solution. The new weights can satisfy the sufficient conditions for optimal order. In fact, the convergence order of the fifth-order WENO (WENO-Z) scheme proposed by Borges et al.[7] at critical points is influenced by the power parameter in the definition of weights, for example, the accuracy is fourth- and fifth-order if the power q takes the value of 1 and 2, respectively. On the other hand, Borges et al. pointed out that, for solutions containing the discontinuities, increasing q makes the scheme more dissipative. The weighting method proposed by Borges at al. provides a straightforward way for improving the performance of a WENO scheme. Castro et al.[8] developed higher-order WENO-Z schemes. Ha et al.[9] introduced a set of different local smoothness indicators (LSIs) for sub-stencils and a sixth-order global smoothness indicator (GSI) ζ to calculate weights, the new WENO-Z-type (WENO-NS) scheme improves the ability of detecting the complicated solution structures. Kim et al.[10] further introduced a parameter to make a balanced tradeoff among the new LSIs of Ha et al.[9], the resulted scheme (WENO-P) yields better results than WENO-NS for problems including discontinuities. Fan et al.[11] constructed several higher-order (up to eighth-order) GSIs, the associated WENO-Z-type schemes (WENO-Zη) can obtain fifth convergence order in smooth regions, even at the second-order critical points where both the first and second derivatives vanish. Hu et al.[12] constructed an adaptive central-upwind WENO scheme (WENO-CU6), in which, a tunable parameter was introduced for the weighting function of WENO-Z to increase the contribution of optimal weights. Acker et al.[13] presented a way of increasing the relevance of less-smooth sub-stencils by adding a new term into the WENO-Z weights, the new scheme (WENO-Z+) improves the resolution of the high-frequency smooth waves. These WENO-Z-type schemes mentioned above successfully improve the accuracy and decrease the dissipation in many problems. However, some of them, such as WENO-NS, WENO-P, WENO-CU6 and WENOZ+ schemes, introduced empirical tunable parameters, and hence their applications are limited. Some of them, such as WENO-Zη schemes, are prone to generate spurious oscillations near shock regions. Although the authors[7, 13] demonstrated that the smaller dissipation of the scheme has more influence than its convergence rate at critical points when solving problems with shocks, how to get both the optimal order at critical points and lower dissipation of a WENO-Z-type scheme is still worthy to study, especially for simulating the complicated flow fields.

In this paper, we propose a new sixth-order global smoothness indicator (GSI-6), and a function consisted of the GSI-6 and local smoothness indicators (IS_k) to calculate the weights of the fifth-order WENO scheme. For a smooth solution, the new weights satisfy the sufficient condition for fifth-order convergence in smooth regions, hence the new scheme performs better than the WENO-Z scheme. While, for discontinuous solutions, the weights of the new scheme assigned to discontinuous sub-stencils are as large as the ones of WENO-Z, i.e, the behavior of the new scheme in shock regions is similar to that of the WENO-Z scheme. Hence, the new scheme performs well for both smooth and discontinuous solutions.

This paper is organized as follows: in Section 2, several WENO schemes are briefly introduced. In Section 3, the new scheme is proposed and a detailed discussion is given. In Section 4, various numerical examples are presented to demonstrate the good performance of the new scheme. Concluding remarks are given in Section 5.

2. THE WENO SCHEMES

In this section, we briefly review the WENO schemes by using the scalar conservative law equation,

$$\frac{\partial u}{\partial t}+\frac{\partial f(u)}{\partial x}=0. \tag{1}$$

As in [6, 7], by defining the points $x_i = i\Delta x$, $(i = 0, \ldots, N)$, where Δx is the uniform grid spacing, (1) can be approximated by a conservative finite difference formula as follows,

$$\frac{du_i}{dt}=-\frac{\hat{f}_{i+1/2}-\hat{f}_{i-1/2}}{\Delta x}, \tag{2}$$

where $\hat{f}_{i\pm1/2}$ are the numerical fluxex.

2.1. The WENO-JS scheme

The flux of a fifth-order WENO[3] scheme can be written as,

$$\hat{f}_{i+1/2}=\sum_{k=0}^{2}\omega_k q_k, \tag{3}$$

where q_k is the third-order flux on the sub-stencil $S_k = (i + k - 2, i + k - 1, i + k)$, and given by,

$$\begin{cases} q_0 = & \frac{1}{3}f_{i-2}-\frac{7}{6}f_{i-1}+\frac{11}{6}f_i, \\ q_1 = & -\frac{1}{6}f_{i-1}+\frac{5}{6}f_i+\frac{1}{3}f_{i+1}, \\ q_2 = & \frac{1}{3}f_i+\frac{5}{6}f_{i+1}-\frac{1}{6}f_{i+2}. \end{cases} \tag{4}$$

The weight function of Jiang and Shu[3] is,

$$\omega_k^{JS}=\frac{\alpha_k}{\alpha_0+\alpha_1+\alpha_2}, \alpha_k=\frac{c_k}{(IS_k+\epsilon)^2}, k=0,1,2, \tag{5}$$

where, IS_k is called as local smoothness indicator (LSI), which is used to measure the relative smoothness of a solution on the sub-stencil S_k. $c_0 = 0.1, c_1 = 0.6$ and $c_2 = 0.3$ are the optimal weights, which generate the fifth-order upstream scheme. ϵ is a positive real number introduced to avoid the denominator becoming zero. Henrick et al. [6] discussed the role of ϵ. To avoid the values of ϵ affecting the ENO behavior, $\epsilon = 10^{-40}$ is suggested by Henrick et al.[6] and also used in this paper.

In [3], Jiang and Shu proposed a classical local smoothness indicator (LSI) as,

$$IS_k=\sum_{l=1}^{r-1}\int_{x_{i-1/2}}^{x_{i+1/2}}(\Delta x)^{2l-1}(q_k^{(l)})^2dx, \tag{6}$$

where, $q_k^{(l)}$ is the lth order derivative of $q_k(x)$, and $q_k(x)$ is the interpolation polynomial on sub-stencil S_k. Shen and Zha[14] suggested using a flexible and simple formula to calculate the LSI,

$$IS_k=\sum_{l=1}^{r-1}\gamma_l[f_k^{(l)}]^2, \tag{7}$$

where $f_k^{(l)}$ is the approximation of the lth derivative $f_{x_i}^{(l)}\Delta x^l$ on sub-stencil S_k. For the fifth-order WENO scheme, $r = 3$, and,

$$\begin{cases} f_0^{(1)}=(f_{i-2}-4f_{i-1}+3f_i)/2, \\ f_1^{(1)}=(-f_{i-1}+f_{i+1})/2, \\ f_2^{(1)}=(-3f_i+4f_{i+1}-f_{i+2})/2, \end{cases} \text{and} \quad \begin{cases} f_0^{(2)}=f_{i-2}-2f_{i-1}+f_i, \\ f_1^{(2)}=f_{i-1}-2f_i+f_{i+1}, \\ f_2^{(2)}=f_i-2f_{i+1}+f_{i+2}. \end{cases} \tag{8}$$

The coefficients γ_1 and γ_2 can choose different values. For example, the formula (6) of Jiang and Shu gives $\gamma_1 = 1$ and $\gamma_2 = 13/12$; Fan et al.[11] used $\gamma_1 = 1$ and $\gamma_2 = 1$. For analyzing conveniently in the next content, the Taylor expansion of IS_k at x_i for a smooth solution is given as following,

$$\begin{cases} IS_0 = & f_i'^2\Delta x^2 + (\frac{13}{12}f_i''^2 - \frac{2}{3}f_i'f_i''')\Delta x^4 + (-\frac{13}{6}f_i''f_i''' + \frac{1}{2}f_i'f_i^{(4)})\Delta x^5 + O(\Delta x^6), \\ IS_1 = & f_i'^2\Delta x^2 + (\frac{13}{12}f_i''^2 + \frac{1}{3}f_i'f_i''')\Delta x^4 + O(\Delta x^6), \\ IS_2 = & f_i'^2\Delta x^2 + (\frac{13}{12}f_i''^2 - \frac{2}{3}f_i'f_i''')\Delta x^4 + (\frac{13}{6}f_i''f_i''' - \frac{1}{2}f_i'f_i^{(4)})\Delta x^5 + O(\Delta x^6). \end{cases} \tag{9}$$

The expansion (9) means that,

$$IS_k = \begin{cases} D_0[1 + O(\Delta x^2)], \ D_0 = f_i'^2\Delta x^2, & f' \neq 0, \\ D_1[1 + O(\Delta x)], \quad D_1 = \frac{13}{12}f_i'''\Delta x^4, & f' = 0. \end{cases} \tag{10}$$

Substituting (10) into (5) gives,

$$\omega_k^{JS} = \begin{cases} c_k + O(\Delta x^2), & f' \neq 0, \\ c_k + O(\Delta x), & f' = 0. \end{cases} \tag{11}$$

In [6], Henrick et al. derived the necessary and sufficient conditions for fifth-order convergence of a fifth-order WENO scheme, and pointed out that the WENO-JS scheme may even decrease to third-order accuracy at critical points, hence a mapping function[6] is proposed to make the new weights satisfy a sufficient condition, which is given as,

$$\omega_k = c_k + O(\Delta x^3). \tag{12}$$

Although it is not necessary, as mentioned by Henrick et al.[6], (12) can serve as a simple criteria to design the weights for fifth-order WENO schemes.

2.2. The WENO-Z scheme

The fifth-order WENO-Z scheme is proposed by Borges et al.[7] by introducing a global smoothness indicator (GSI) τ to calculate the weights,

$$\omega_k^Z = \frac{\alpha_k}{\alpha_0 + \alpha_1 + \alpha_2}, \ \alpha_k = c_k\left(1 + (\frac{\tau}{IS_k + \epsilon})^q\right). \tag{13}$$

The original GSI of Borges et al. is,

$$\tau_5 = |IS_2 - IS_0|. \tag{14}$$

Applying the Taylor expansion of IS_k (9), there is,

$$\tau_5 = \left|\frac{13}{3}f''f''' - f'f^{(4)}\right|\Delta x^5 + O(\Delta x^6). \tag{15}$$

Hence, one can get,

$$\omega_k^Z = \begin{cases} c_k + O(\Delta x^{3q}), & f_i' \neq 0, \\ c_k + O(\Delta x^q), & f_i' = 0, \end{cases} \tag{16}$$

where q is a tunable parameter. Numerical results in [7] demonstrated that, if q takes 1, the accuracy order at critical points is only fourth; with $q = 2$, the scheme can achieve fifth-order accuracy. Meanwhile, Borges et al. pointed out that, for a solution containing the discontinuities, increasing q makes the scheme more dissipative, and the smaller dissipation of WENO-Z has much more influence than its rate of convergence at critical points when solving problems with shocks. Hence, $q = 1$ is suggested for the WENO-Z scheme in [7].

2.3. Several improved WENO-Z-type schemes

The weight function (13) of the WENO-Z scheme provides a straight-forward method for improving the accuracy of a WENO scheme. Here, several improved WENO-Z-type schemes are briefly introduced.

WENO-NS: Ha et al.[9] constructed a sixth-order global smoothness indicator(GSI) as,

$$\zeta = \frac{1}{2}\left(|\beta_0 - \beta_2|^2 + g(|L_{1,1}f|)^2\right), g(x) = \frac{x^3}{1+x^3}, \tag{17}$$

where, $\beta_k = \xi|L_{1,k}f| + |L_{2,k}f|$ takes the similar expression as (7), in which ξ is a tunable parameter and $L_{l,k}f$ is the approximation of the lth derivative $f^{(l)}_{i+1/2}$ on sub-stencil S_k, and the local smoothness indicator (LSI) IS_k is calculated as $IS_k = \beta_k^2$.

WENO-P: To save the computational cost, Kim et al.[10] simplified the sixth-order GSI (17) as,

$$\zeta = (\beta_0 - \beta_2)^2, \tag{18}$$

and introduced a parameter δ to make a balanced contribution of the β_k of Ha et al. as,

$$\tilde{\beta_0} = \beta_0,\ \tilde{\beta_1} = (1+\delta)\beta_1,\ \tilde{\beta_2} = (1-\delta)\beta_2. \tag{19}$$

WENO-Zη: Fan et al.[11] proposed a sixth-order GSI as,

$$\tau_6 = |\eta_5 - \frac{IS_0 + 4IS_1 + IS_2}{6}|, \tag{20}$$

and two eighth-order GSIs as,

$$\begin{aligned} \tau_{81} &= |(|f_0^1| - |f_2^1|)(f_0^2 + f_2^2 - 2f_1^2)|, \\ \tau_{82} &= (|f_0^1| - |f_2^1|)^2 + (f_0^2 + f_2^2 - 2f_1^2)^2, \end{aligned} \tag{21}$$

where, $\eta_5 = \frac{1}{144}[(f_{i-2} - 8f_{i-1} + 8f_{i+1} - f_{i+2})^2 + (f_{i-2} - 16f_{i-1} + 30f_i - 16f_{i+1} + f_{i+2})^2]$, and the IS_k (7) with $\gamma_1 = \gamma_2 = 1$ is used.

WENO-Z+: Acker et al.[13] proposed a way of improving the results of WENO-Z by increasing the weights of less-smooth sub-stencils,

$$\alpha_k = c_k\left[1 + \left(\frac{\tau_5 + \epsilon}{IS_k + \epsilon}\right)^2 + \lambda\left(\frac{IS_k + \epsilon}{\tau_5 + \epsilon}\right)\right], \tag{22}$$

where λ is a parameter being dependent on the grid spacing.

WENO-CU6: Hu et al.[12] constructed an adaptive central-upwind WENO scheme, in which, the weights are constructed as,

$$\omega_k = \frac{\alpha_k}{\sum_{k=0}^{k=3}\alpha_k},\ \alpha_k = c_k\left(C + \frac{\tau_6}{IS_k + \epsilon}\right), \tag{23}$$

where, IS_3 is the smoothness indicator (6) on the stencil $S^6 = (i-2, \cdots, i+3)$, and $\tau_6 = |IS_3 - (IS_0 + 4IS_1 + IS_2)/6|$. The parameter C ($C = 20$ is suggested in [12]) is introduced to increase the contribution of optimal weights and decrease the numerical dissipation.

Numerical results showed that the improved WENO-Z-type schemes mentioned above perform well in most of the tested cases. However, those parameters, such as ξ in (17) and (18), δ in (19), C in (23) and λ in (22), are problem-dependent and chosen empirically, and the WENO-Zη schemes (use high order GSIs (21)) are prone to generate oscillations near discontinuities. Hence the applications of these schemes to complex flow fields are greatly limited.

3. THE NEW WENO SCHEME

In this section, we propose a new method to improve the accuracy of the WENO-Z scheme at critical points while keeping the ENO property near discontinuities.

3.1. The new weighting method

First, a new global smoothness indicator (GSI) is designed as,

$$\tau_6' = \gamma_1(|f_0^{(1)}| - |f_2^{(1)}|)^2 + \gamma_2(|f_0^{(2)}| - |f_2^{(2)}|)^2, \tag{24}$$

where, the parameters γ_1 and γ_2 are the same as used for IS_k(7), in this paper, they take the same values ($\gamma_1 = 1$ and $\gamma_2 = 13/12$) as those of Jiang and Shu[3]. It should be pointed out, since $f_k^{(l)}$ is required to calculate LSI IS_k (7), τ_6' has only a few operations more than τ_5 (14).

Then, a new method for calculating the weights is proposed as,

$$\omega_k^{ZA} = \frac{\alpha_k}{\alpha_0 + \alpha_1 + \alpha_2},\ \alpha_k = c_k\left(1 + \frac{A \cdot \tau_6'}{IS_k + \epsilon}\right), \tag{25}$$

where, the function A is suggested as,

$$A = \frac{\tau_6'}{IS_0 + IS_2 - \tau_6' + \epsilon}. \tag{26}$$

Clearly, there is,

$$\tau_6' \leq \gamma_1\left[f_0^{(1)}\right]^2 + \gamma_2\left[f_0^{(2)})\right]^2 + \gamma_1\left[f_2^{(1)}\right]^2 + \gamma_2\left[f_2^{(2)})\right]^2 = IS_0 + IS_2, \tag{27}$$

hence, $IS_0 + IS_2 - \tau_6' \geq 0$ and $A > 0$.

3.2. The properties of the new weights

Next, we discuss the accuracy of the new weights in smooth regions and their behaviors near discontinuities.

For a smooth global stencil, by means of the Taylor series expansion and simple derivation, one can get,

$$\begin{aligned}\tau_6' \leq \gamma_1(f_0^{(1)} - f_2^{(1)})^2 + \gamma_2(f_0^{(2)} - f_2^{(2)})^2 =& (\frac{1}{4}f_i^{(4)}(\Delta x)^4 + O(\Delta x)^6)^2 + (\frac{13}{6}f_i'''(\Delta x)^3 + O(\Delta x)^5)^2 \\ =& O(\Delta x^6).\end{aligned} \tag{28}$$

Then, substituting (9) and (28) into (26), one can easily find that,

$$A = \begin{cases} O(\Delta x^4), & f_i' \neq 0, \\ O(\Delta x^2), & f_i' = 0. \end{cases} \tag{29}$$

Using the definition of the weights (25), it is obtained that,

$$\omega_k^{ZA} = c_k + O\left(\frac{A \cdot \tau_6'}{IS_k + \epsilon}\right) = \begin{cases} c_k + O(\Delta x^8) & , f_i' \neq 0, \\ c_k + O(\Delta x^4) & , f_i' = 0. \end{cases} \tag{30}$$

Formula (30) implies that the new weights go beyond the sufficient condition (12), and hence the fifth-order accuracy is guaranteed, including at critical points ($f_i' = 0$).

If the solution is discontinuous on a global stencil, without loss of generality, assume that the sub-stencil S_0 contains the discontinuity and S_2 is smooth, then there is, $IS_0 \gg IS_2$, and,

$$\tau_6' \approx IS_0 \gg IS_2, \text{and, } A \gg 1. \tag{31}$$

Thus, α_k in (25) can be approximated by,

$$\alpha_k = A \cdot c_k \left(\frac{1}{A} + \frac{\tau_6'}{IS_k + \epsilon} \right) \simeq A \cdot \tau_6' \left(\frac{c_k}{IS_k + \epsilon} \right). \tag{32}$$

That means, the regularized weights (ω_k^{ZA}) are mainly determined by the local smoothness indicator IS_k.Hence, the ENO property of the new scheme can be preserved well.

In addition, using the expression of function A (26), α_k in (25) can also be written as,

$$\alpha_k = c_k \left(1 + \left(\frac{IS_k + \epsilon}{IS_0 + IS_2 - \tau_6' + \epsilon} \right) \left(\frac{\tau_6'}{IS_k + \epsilon} \right)^2 \right). \tag{33}$$

For a smooth stencil,

$$\frac{IS_k + \epsilon}{IS_0 + IS_2 - \tau_6' + \epsilon} = \begin{cases} \frac{1}{2} + O(\Delta x^4), f_i' \neq 0, \\ \frac{1}{2} + O(\Delta x^2), f_i' = 0. \end{cases} \tag{34}$$

Hence, the new scheme has the same accuracy order (fifth order) as the weighted scheme with,

$$\alpha_k = c_k \left(1 + (\frac{\tau_6'}{IS_k + \epsilon})^2 \right). \tag{35}$$

From above analysis, we can conclude that, the new scheme has low dissipation as the WENO-Z-type scheme with $q = 1$ on the discontinuous stencil and is fifth order convergence as the WENO-Z-type scheme with $q = 2$ on the smooth stencil. For convenience, the WENO-Z-type scheme with τ_6' (24) is denoted as WENO-Zτ_6', and the new scheme (25) is denoted as WENO-ZA.

It is worth to note that, the self-adaptive function A is very different from the tuning parameter C [12]. For smooth solutions, A is much smaller than 1 ($A \ll 1$) and it plays a similar role in the weights as a large constant C introduced in (23) does; but for solutions containing discontinuities, large C may generate oscillation and instability[12], while A is much larger than 1 ($A \gg 1$) and its effect similar to a small C, as shown in (32), hence the ENO properties can be preserved well.

As a matter of fact, $(A \cdot \tau_6')$ can be regarded as a global smoothness indicator τ_8', which is independent of k and has the same dimension as IS_k. From (28) and (29), there is,

$$\tau_8' = A \cdot \tau_6' = \begin{cases} O(\Delta x^{10}), & f_i' \neq 0, \\ O(\Delta x^8), & f_i' = 0. \end{cases} \tag{36}$$

3.3. The dispersion and dissipation properties of the WENO-ZA scheme

In this sub-section, the dispersion and dissipation properties of the present scheme are investigated by analysing its spectral properties. The representation for the approximate dispersion relation of linear and non-linear finite-difference schemes can be found in [15]. As shown in Fig. 1, compared with the WENO-Z scheme, the present scheme improves both the dispersion and dissipation errors effectively.

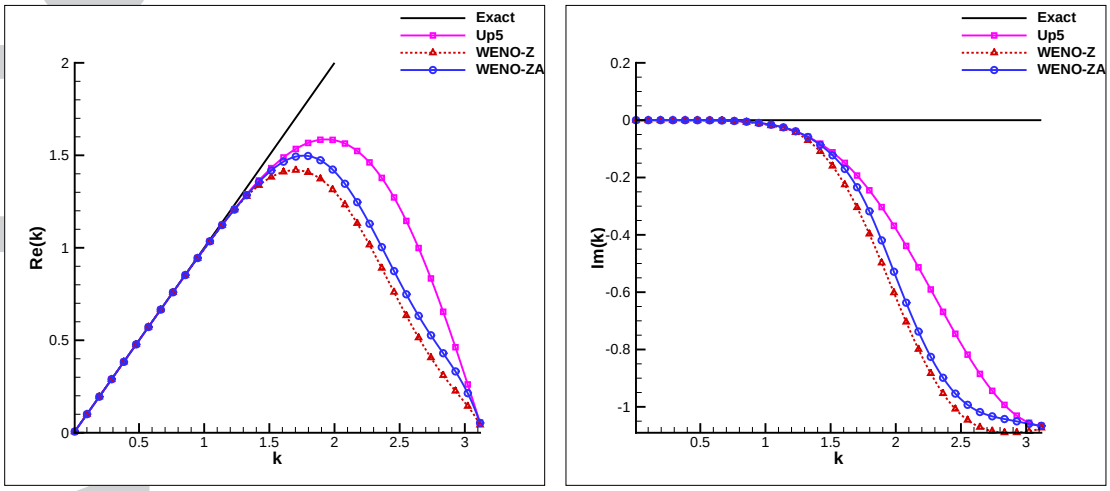

(a) Dispersion (b) Dissipation

Figure 1. The dispersion and dissipation properties

4. NUMERICAL EXAMPLES

In this section, several linear advection problems, one- and two-dimensional Euler problems are calculated, and in order to show the good performance of the new scheme, the following schemes are compared,

(1) WENO-Z[7]: GSI τ_5 (14) and $q = 1$;
(2) WENO-Z2[7]: GSI τ_5 (14) and $q = 2$;
(3) WENO-NS[9]: GSI ζ (17) and $\xi = 0.1$ for linear problems, $\xi = 0.4$ for non-linear problems;
(4) WENO-P[10]: GSI ζ (18) and $\delta = 0.05$;
(5) WENO-Zη[11]: GSIs are τ_6 (20), τ_{81} and τ_{82} (21), respectively, and $q = 1$;
(6) WENO-Z+[13]: weighting method (22) and GSI τ_5 (14), and $\lambda = \Delta x^{2/3}$;
(7) WENO-Zτ_6': GSI τ_6' (24) and $q = 1$;
(8) WENO-Zτ_6'2: GSI τ_6' (24) and $q = 2$;
(9) WENO-ZA: weighting method (25) and GSI τ_6' (24).

For convenience, the purpose of these comparisons are outlined here,

(1) Testing WENO-Zτ_6' (See Table.I and Fig.8) is to show that, comparing to other GSIs, τ_6' is a compromise GSI, which can keep the ENO property and achieve high order accuracy simultaneously.

(2) Testing WENO-Z2 and WENO-τ_6'2 (See Table.I and Figs.4 and 8) is to show that, comparing the power $q = 1$, $q = 2$ can improve the accuracy order for smooth solution, but it really increases the numerical dissipation near discontinuities.

(3) The comparisons of WENO-τ_6', WENO-τ_6'2 and WENO-ZA (See Table.I and Figs.4 and 9) are used to show that the new weighting method (25) is necessary and valuable for both improving the accuracy in smooth regions and decreasing the dissipation near discontinuities.

(4) The comparisons of WENO-ZA, WENO-Z, WENO-Zη, WENO-NS and WENO-P (See Sections 4.1-4.3) are used to show that the comprehensive advantages of WENO-ZA over the others, including ENO property, high-order accuracy, high resolution, and low dissipation.

In this paper, time advancement is performed with the fourth-order Runge-Kutta method[16].

4.1. The convergence rate at critical point

The function $f(x) = x^3 + \cos(x)$ is used to test the numerical convergence order of different schemes. At $x = 0$, there is $f'_{x=0} = 0$ and $f'''_{x=0} \neq 0$. As shown in Table I, the WENO-Z scheme and WENO-P scheme only get fourth order accuracy. The WENO-Z2, WENO-NS, WENO-Zη(τ_6),

WENO-Z$\eta(\tau_{81})$, WENO-Zτ_6', WENO-Z$\tau_6'2$ and WENO-ZA schemes get fifth order accuracy, but only WENO-Z$\eta(\tau_{81})$, WENO-Z$\tau_6'2$ and the WENO-ZA schemes can obtain the errors with the same order of magnitude as those of the fifth-order upstream (Up5) scheme, and the errors generated by the other schemes are at least three orders of magnitude larger than those of the WENO-ZA scheme. WENO-Z$\eta(\tau_{82})$ has similar results as WENO-Z$\eta(\tau_{81})$, and hence is not shown in this Table.

It should be noted that, for this case, the WENO-Z+ scheme can only obtain third order accuracy as well as the WENO-JS scheme. In addition, since the parameter λ is dependent on the grid spacing, the resulting WENO-Z+ scheme no longer preserves the scale invariance. This shortcoming greatly limits the applications of WENO-Z+. For the WENO-P scheme, the parameter δ in (19) generates different coefficients in different IS_k, hence the accuracy rate is influenced.

As the results of the WENO-Zτ_6' and WENO-Z$\tau_6'2$ schemes shown, WENO-Zτ_6' obtains similar results as the WENO-Z2 scheme, since at critical point, there are $\tau_6'/(IS_k+\epsilon) = O(\Delta x^2)$ and $[\tau_5/(IS_k+\epsilon)]^2 = O(\Delta x^2)$. In addition, as analyzed in Sec 3.2, for the smooth solution, the WENO-Z$\tau_6'2$ scheme obtains almost the same errors as the new scheme with function A (WENO-ZA).

Table I. Convergence order at the critical point

Δx	Up5		WENO-JS		WENO-Z		WENO-Z2	
	error	order	error	order	error	order	error	order
5.00E-3	5.208E-14	-	1.566E-07	-	4.133E-09	-	1.118E-10	-
2.50E-3	1.628E-15	5.000	2.323E-08	2.752	3.353E-10	3.624	1.128E-11	3.309
1.25E-3	5.086E-17	5.000	3.138E-09	2.888	2.357E-11	3.831	5.866E-13	4.266
6.25E-4	1.589E-18	5.000	4.070E-10	2.947	1.558E-12	3.919	2.200E-14	4.737
3.12E-4	4.967E-20	5.000	5.180E-11	2.974	1.001E-13	3.960	7.448E-16	4.884

Δx	WENO-NS		WENO-P		WENO-Z$\eta(\tau_6)$		WENO-Z$\eta(\tau_{81})$	
5.00E-3	5.266E-11	-	8.233E-10	-	1.142E-11	-	5.209E-14	-
2.50E-3	1.938E-12	4.764	4.776E-11	4.108	4.756E-13	4.586	1.628E-15	5.000
1.25E-3	6.472E-14	4.905	2.892E-12	4.046	1.672E-14	4.830	5.086E-17	5.000
6.25E-3	2.084E-15	4.957	1.782E-13	4.021	5.518E-16	4.922	1.589E-18	5.000
3.12E-3	6.604E-17	4.980	1.106E-14	4.010	1.770E-17	4.962	4.967E-20	5.000

Δx	WENO-Z+		WENO-Zτ_6'		WENO-Z$\tau_6'2$		WENO-ZA	
5.00E-3	3.417E-08	-	1.217E-10	-	1.039E-13	-	9.634E-14	-
2.50E-3	4.975E-09	2.780	5.059E-12	4.589	3.979E-15	4.706	2.539E-15	5.246
1.25E-3	7.174E-10	2.794	1.778E-13	4.831	8.315E-17	5.581	6.019E-17	5.398
6.25E-3	1.019E-10	2.816	5.863E-15	4.922	1.896E-18	5.455	1.671E-18	5.171
3.12E-3	1.427E-11	2.836	1.880E-16	4.963	5.228E-20	5.181	5.034E-20	5.053

4.2. Linear advection problems

In this sub-section, the linear advection equation (37) is solved to compare the shock-capturing ability, robustness and the low dissipation property of different schemes.

$$\begin{cases} \dfrac{\partial u}{\partial t} + \dfrac{\partial u}{\partial x} = 0, & x_0 \leqslant x \leqslant x_1, \\ u(x, t=0) = u_0(x), & \text{periodic boundary}. \end{cases} \tag{37}$$

The exact solution of (37) is $u(x,t) = u_0(x-t)$.

*4.2.1. Case 1 * linear problem with a discontinuity*

$$u_0(x) = \begin{cases} -\sin(\pi x) - \frac{1}{2}x^3, & -1 \leq x < 0, \\ -\sin(\pi x) - \frac{1}{2}x^3 + 1, & 0 \leq x \leq 1. \end{cases} \tag{38}$$

First, the solution, which contains a discontinuity at $x = 0$, is used to show the behavior of the new GSI $\tau_8' = A \cdot \tau_6'$ (36) in the smooth regions and discontinuous regions. Fig.2 is the distribution of the

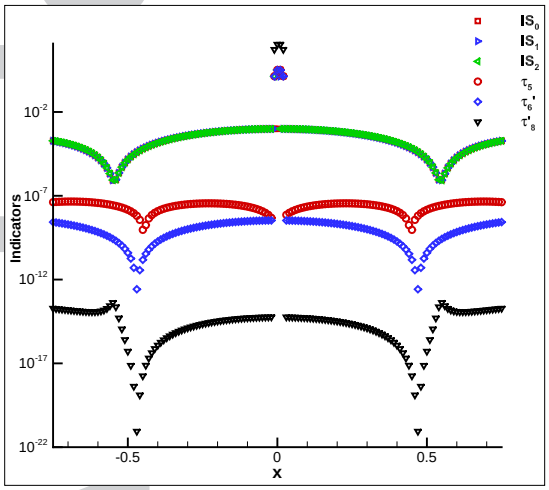

Figure 2. Distribution of LSIs and GSIs at $t = 0$

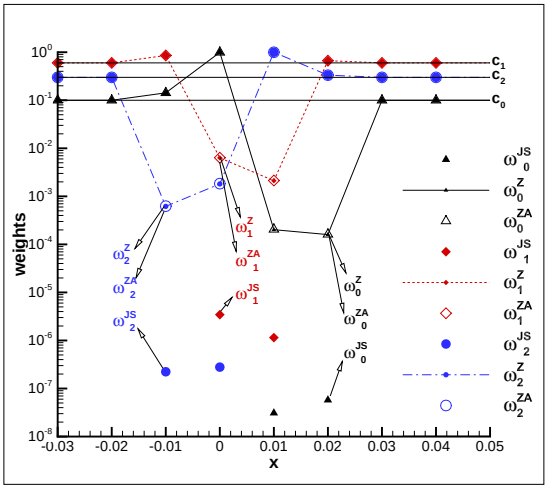

Figure 3. Distribution of weights near discontinuity

local smoothness indicators IS_k and three global smoothness indicators (GSIs), τ_5, τ_6' and τ_8', for the initial solution. As shown in Fig.2, the value of τ_8' is the smallest one in smooth regions, which indicates that τ_8' is an infinitesimal with higher order than τ_5 and τ_6', and hence the new scheme is more accurate than WENO-Z. Although τ_8' is larger than the others near discontinuity, it does not break the ENO property, as illustrated in (32). And Fig.3 shows that, near discontinuity, the weights of the new scheme are almost the same as those of WENO-Z, both of them assign larger weights to sub-stencils containing discontinuity than WENO-JS(for example, see ω_2^{JS}, ω_2^{Z} and ω_2^{ZA}). Hence, as Borges et al.[7] pointed out, for the solution containing discontinuities, WENO-Z is less dissipative than WENO-JS due to the relative large weights assigned to the sub-stencils containing discontinuities, and the same holds for the present scheme.

The numerical results at $t = 2$ with $N = 200$ and $\Delta t = \Delta x/2$ are plotted in Fig. 4. Near discontinuity, the new scheme shows less dissipation than the WENO-Z$\tau_6'2$ scheme, and it is closer to the WENO-Zτ_6'. This also indicates that the power $q = 2$ brings larger dissipation than $q = 1$, and the present weighting method (WENO-ZA) is effective in decreasing dissipation near discontinuities..

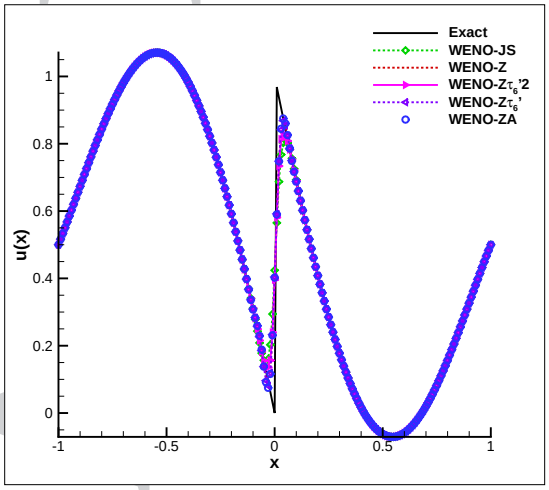

(a)

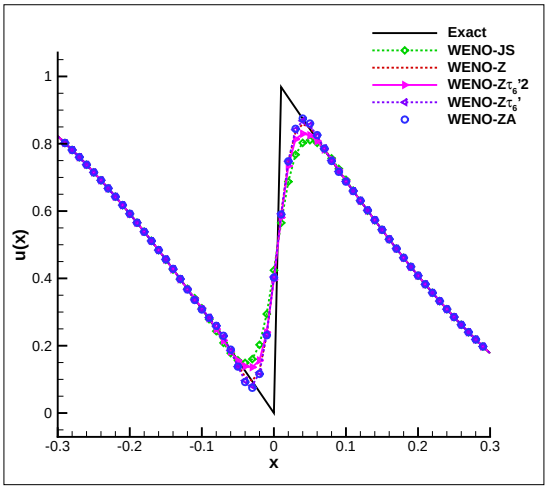

(b)

Figure 4. Case 1, $t = 2$, $N = 200$, using WENO-JS, WENO-Z, WNEO-Z$\tau_6'2$ and WENO-ZA

*4.2.2. Case 2 * linear problem to test the accuracy*

$$u_0(x) = \sin(\pi x - \frac{\sin(\pi x)}{\pi}), -1 \le x \le 1 \tag{39}$$

This solution [6] is often used to test the convergence order in L_∞ norm of WENO schemes. The errors, orders and CPU time of the Up5, WENO-Z and WENO-ZA schemes are compared in Table II. The time step $\Delta t = \Delta x^{5/4}$ is chosen, and the Fortran 95 program with quadruple-precision is performed on Intel Xeon E5-2609 V4. As shown in this table, the WENO-ZA scheme gets fifth order accuracy as the Up5 scheme does, but the WENO-Z scheme fails. Fig. 5 gives the comparisons of computational efficiency. It can be seen that, WENO-ZA costs about 10% CPU time more than WENO-Z, however, if high accuracy (for example, $L_\infty < 1 \times 10^{-8}$ for this case) is required, the new scheme is more efficient than the WENO-Z scheme.

Table II. L_∞ errors, orders and CPU times of Case 2 at $t = 2$

N	Up5			WENO-Z			WENO-ZA		
	error	order	time(ratio)	error	order	time(ratio)	error	order	time(ratio)
80	6.701E-06	-	1.404E-01(0.31)	6.677E-06	-	4.524E-01(1)	6.701E-06	-	4.680E-01(1.03)
160	2.099E-07	5.00	7.176E-01(0.35)	2.099E-07	4.99	2.075E+00(1)	2.099E-07	5.00	2.293E+00(1.11)
320	6.553E-09	5.00	2.668E+00(0.29)	7.767E-09	4.76	9.282E+00(1)	6.552E-09	5.00	1.025E+01(1.10)
640	2.046E-10	5.00	1.260E+01(0.30)	3.570E-10	4.44	4.256E+01(1)	2.046E-10	5.00	4.699E+01(1.10)
1280	6.392E-12	5.00	6.004E+01(0.30)	1.725E-11	4.37	2.013E+02(1)	6.392E-12	5.00	2.223E+02(1.10)

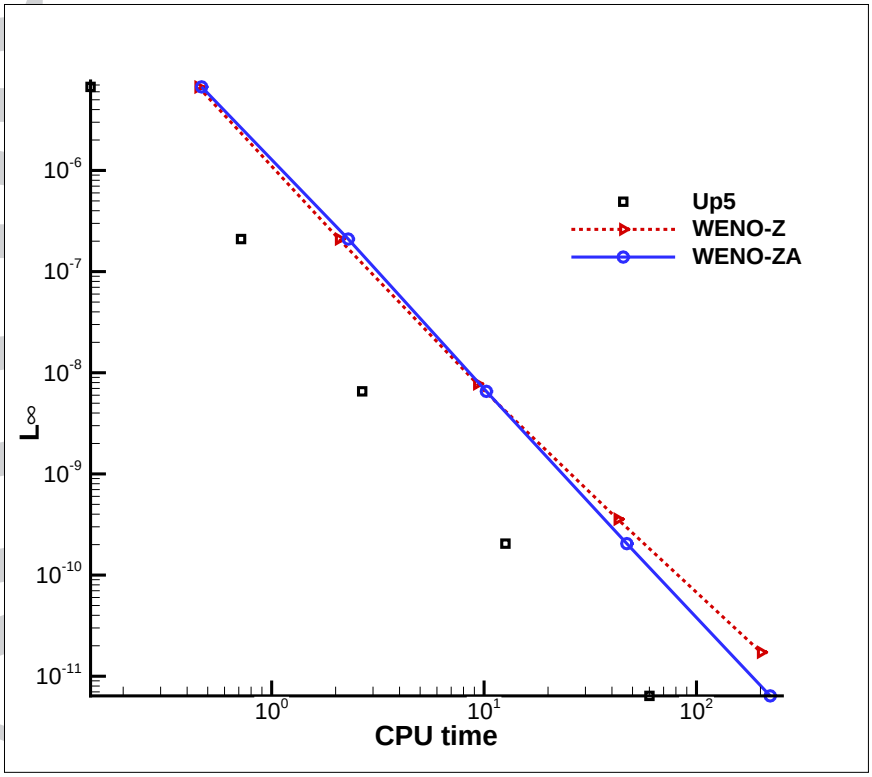

Figure 5. Comparison of the computational efficiency

*4.2.3. Case 3 * linear problem with several critical points*

$$u_0(x) = e^{-(x-90)^2/400}\left(cos\left(\frac{\pi}{8}(x-90)\right) + cos\left(\frac{\pi}{4}(x-90)\right)\right), 50 \le x \le 130 \qquad (40)$$

This smooth solution containing several critical points is used to test the accuracy and numerical dissipation of different schemes. The numerical solutions at $t = 400$ are calculated with $N = 100$ and $\Delta t = \Delta x/2$. As shown in Fig.6, the WENO-ZA scheme obtains almost the same results as Up5, it behaves much better than WENO-Z. The results computed by the WENO-NS, WENO-P and WENO-Zη schemes are also shown in Fig.7. The results of the WENO-Zη schemes (with high order GSIs τ_6, τ_{81} and τ_{82}) are closer to that of WENO-ZA. While, due to the unbalanced contribution provided by three sub-stencils in the WENO-NS and WENO-P schemes [10], both of them generate other issues, such as overestimated extremum, obvious phase error.

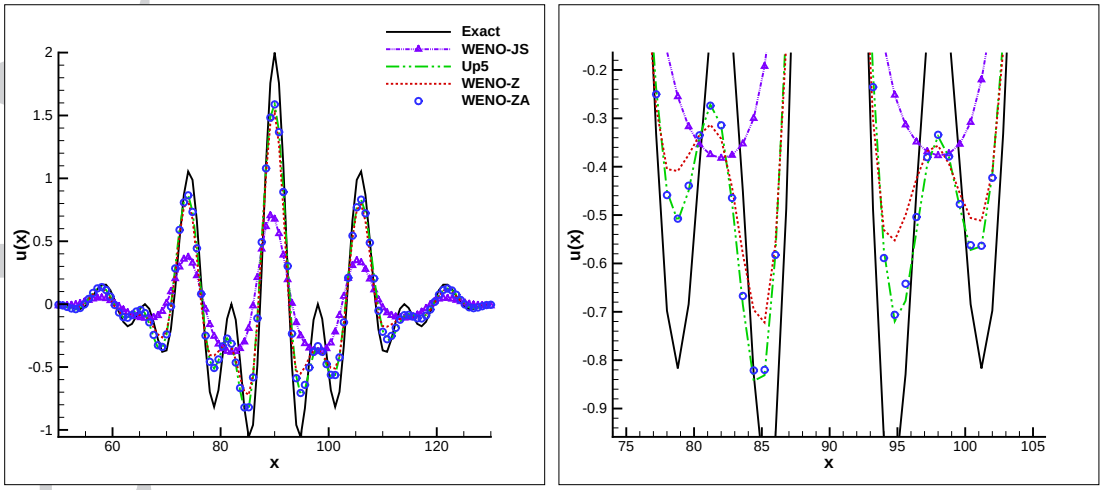

(a) (b)

Figure 6. Case 3, $t = 400$, $N = 100$, using WENO-JS, WENO-Z, Up5 and WENO-ZA

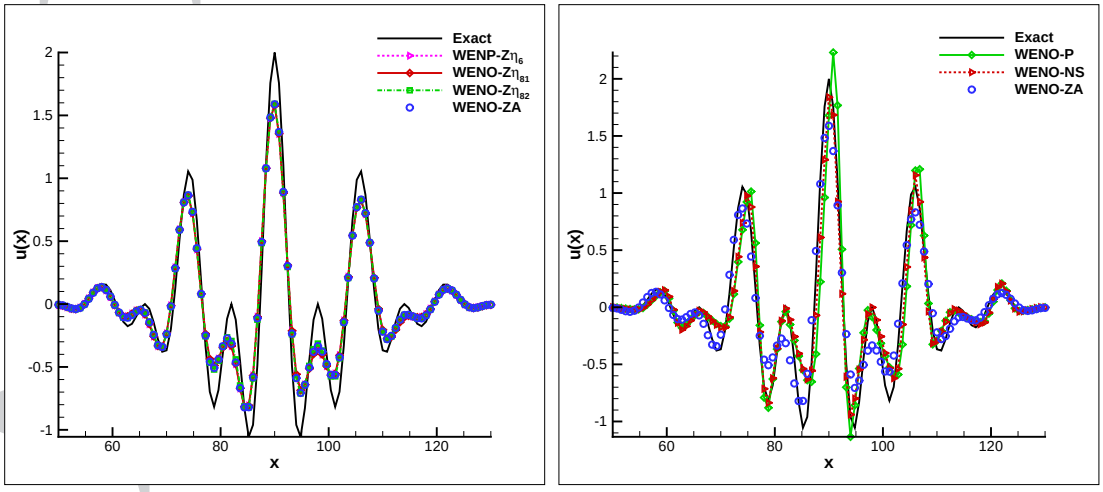

(a) (b)

Figure 7. Case 3, $t = 400$, $N = 100$, using WENO-Zη, WENO-NS, WENO-P and WENO-ZA

*4.2.4. Case 4 * combine-wave problem*

$$u(x,0)=\begin{cases}\frac{1}{6}(G(x,\beta,z-\delta)+G(x,\beta,z+\delta)+4G(x,\beta,z)), & -0.8\leqslant x<-0.6,\\ 1, & -0.4\leqslant x<-0.2,\\ 1-|10(x-0.1)|, & 0\leqslant x<0.2,\\ \frac{1}{6}(F(x,\alpha,a-\delta)+F(x,\alpha,a+\delta)+4F(x,\alpha,a)), & 0.4\leqslant x<0.6,\\ 0, & \text{otherwise},\end{cases}$$

$$G(x,\beta,z)=e^{-\beta(x-z)^2},\ F(x,\alpha,a)=\sqrt{\max(1-\alpha^2(x-a)^2,0)}. \tag{41}$$

The solution consisting of a Gaussian, a triangle, a square-wave and a semi-ellipse wave, is calculated to validate the robustness of different schemes. The constants are $z=-0.7,\ \delta=0.005,\ \beta=ln(2)/(36\delta^2),\ a=0.5$ and $\alpha=10$. It is solved until $t=10$ with $N=200$ and $\Delta t=\Delta x/2$.

The results of the WENO-Zτ_6', WENO-Zτ_6'2 and WENO-Z$\eta(\tau_6)$ are compared in Fig.8. As shown in previous cases, the power $q=2$ (WENO-Zτ_6'2) generates larger dissipation than $q=1$(WENO-Zτ_6'). The GSI τ_6 (WENO-Zτ_6, [11]) obtains clear overestimated and dissymmetric solutions.

The comparisons of WENO-Z, WENO-Zτ_6' and WENO-ZA are given in Fig.9. From the enlarged parts (Fig.9(b)), it can be seen that, WENO-ZA shows less dissipation than the other two schemes.

The results of the WENO-Zη, WENO-NS and WENO-P schemes are also plotted in Figs.10 and 11. As we can see that, the WENO-Zη schemes (with higher-order GSIs τ_{81} and τ_{82}) prone to generate oscillatory solutions near the discontinuities, the WENO-NS and WENO-P scheme obtain overshoot Gaussian wave and dissymmetric semi-ellipse wave, and they also generate larger dissipation for the square wave than WENO-ZA.

From the comparisons of above cases, we can conclude that,

(1) τ_6' (24) proposed in this paper is a compromise GSI, which can keep the ENO property and achieve high order accuracy simultaneously;

(2) the new weighting method (25) is necessary and valuable for both improving the accuracy in smooth regions and decreasing the dissipation near discontinuities.

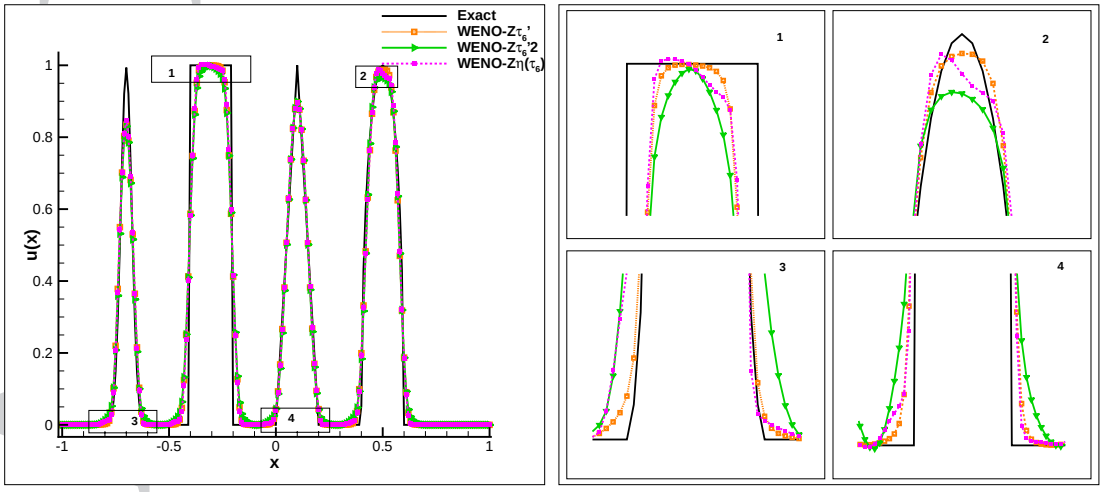

(a) (b)

Figure 8. Case 4, $t=10$, $N=200$, using WENO-Z$\eta(\tau_6)$, WENO-Zτ_6' and WENO-Zτ_6'2

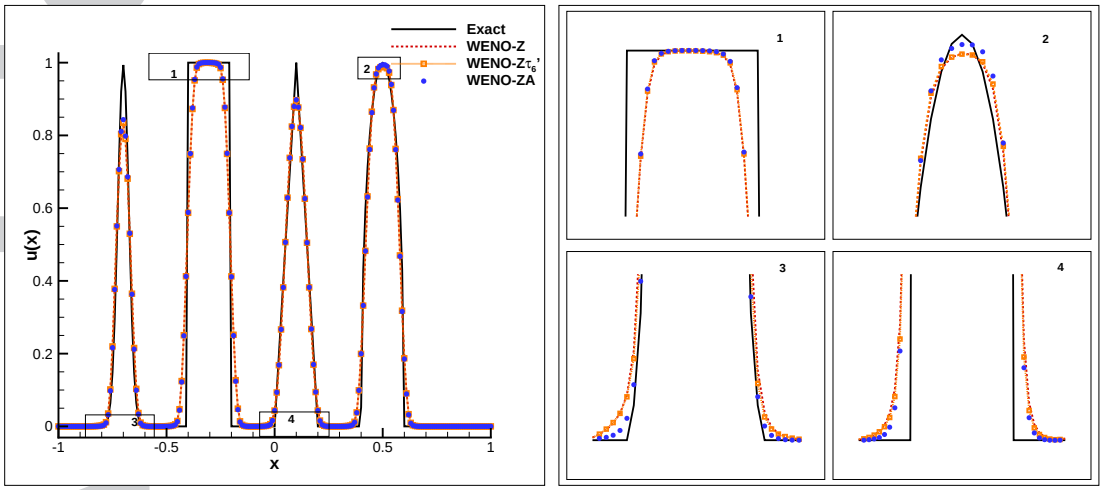

(a) (b)

Figure 9. Case 4, $t = 10$, $N = 200$, using WENO-Z, WENO-Zτ_6' and WENO-ZA

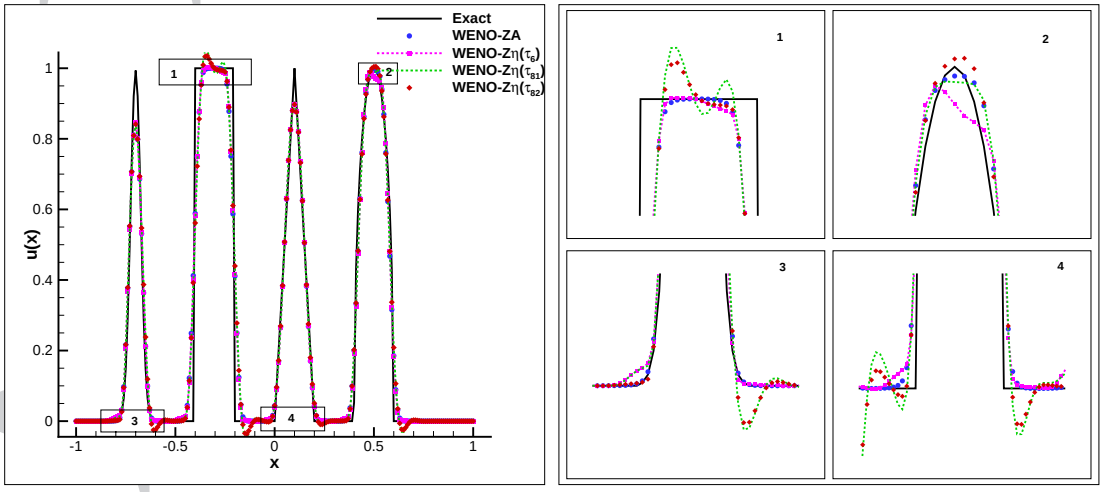

(a) (b)

Figure 10. Case 4, $t = 10$, $N = 200$, using WENO-Zη and WENO-ZA

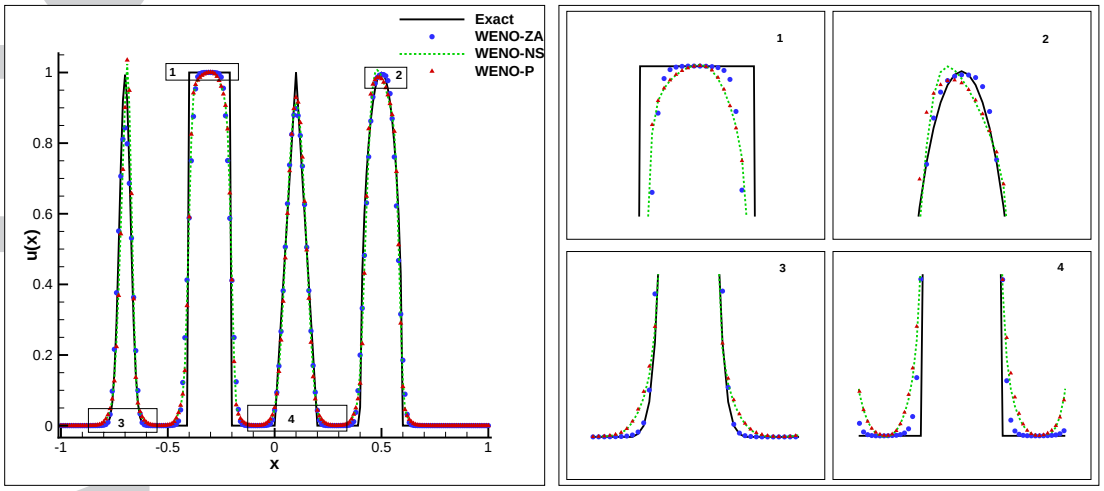

(a) (b)

Figure 11. Case 4, $t = 10$, $N = 200$, using WENO-NS, WENO-P and WENO-ZA

4.3. One-dimensional Euler problems

Next, we further study the behaviors of the WENO-ZA scheme in the one-dimensional Euler problems. The governing equations are as follows,

$$\frac{\partial U}{\partial t} + \frac{\partial F}{\partial x} = 0, \tag{42}$$

where $U = (\rho, \rho u, E)^T$, $F(U) = \left(\rho u, \rho u^2 + p, u(E + p)\right)^T$, ρ, u, E and p are density, velocity, total energy and pressure, respectively,and for ideal gas $E = \dfrac{p}{\gamma - 1} + \dfrac{1}{2}\rho u^2$, $\gamma = 1.4$ is the ratio of specific heat. Time step is taken as,

$$\Delta t = \frac{\sigma \Delta x}{max_i \left(|u_i| + c_i\right)}, \tag{43}$$

where, $\sigma = 0.5$ is CFL number. c is the speed of sound and given by $c = \sqrt{\gamma p/\rho}$. The characteristic-wise Roe-type decomposition method[17] is used for the local characteristic reconstruction. All the reference solutions were obtained by the WENO-Z scheme with a grid of 2000.

*4.3.1. Case 5 * Shu-Osher problem*

The first 1-D case is the Shu-Osher problem[16], with the initial conditions,

$$(\rho, u, p) = \begin{cases} (3.857143,\ 2.629369,\ 31/3), & -5 \le x < -4, \\ (1 + 0.2\sin(5x),\ 0,\ 1), & -4 \le x \le 5. \end{cases} \tag{44}$$

It is ofen used as a benchmark case to test the performance of different schemes. Figs.12 - 14 give the distributions of density at $t = 1.8$ with $N = 200$. As these figures shown, the WENO-ZA scheme is less dissipative than WENO-Z (Fig.12), and it is also comparable with those improved schemes (such as WENO-Zη, WENO-NS and WENO-P). However, although WENO-Zη, WENO-NS and WENO-P can resolve this kind of high frequency wave structure well, their dissipation is not large enough to suppress the oscillations in some problems with strong shock, for example, they even can not finish the calculation of the blast-waves interaction problem in next case. Applications to current case and the next case show the conclusion again, i.e., the WENO-ZA scheme proposed in this paper can keep the ENO property and has high accuracy, low dissipation, simultaneously.

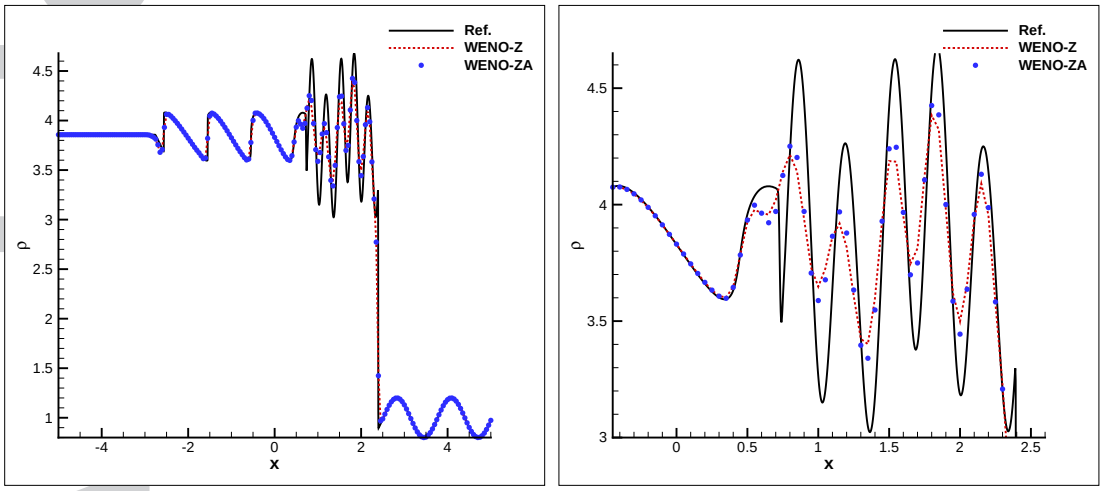

Figure 12. Shu-Osher problem, $t = 1.8$, $N = 200$, using WENO-Z and WENO-ZA

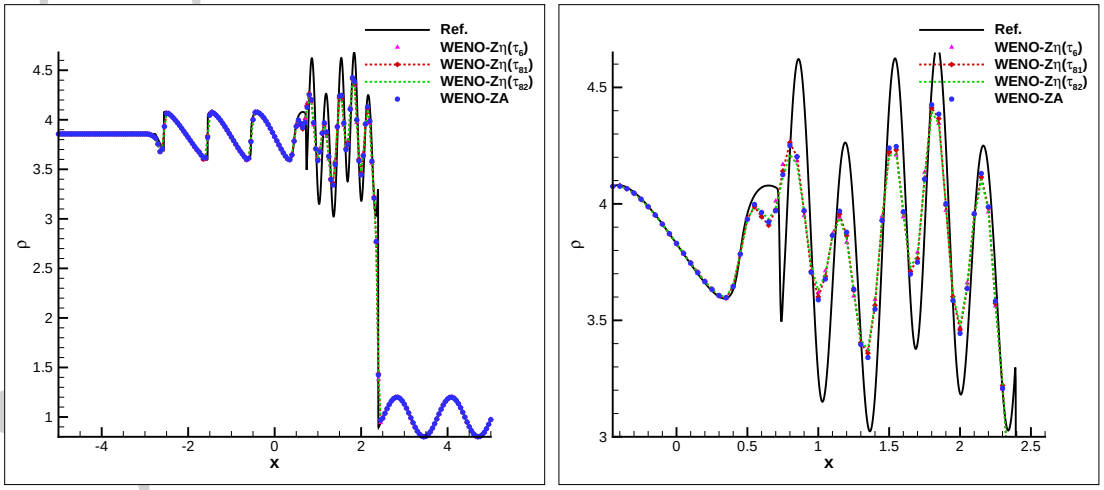

Figure 13. Shu-Osher problem, $t = 1.8$, $N = 200$, using WENO-Zη and WENO-ZA

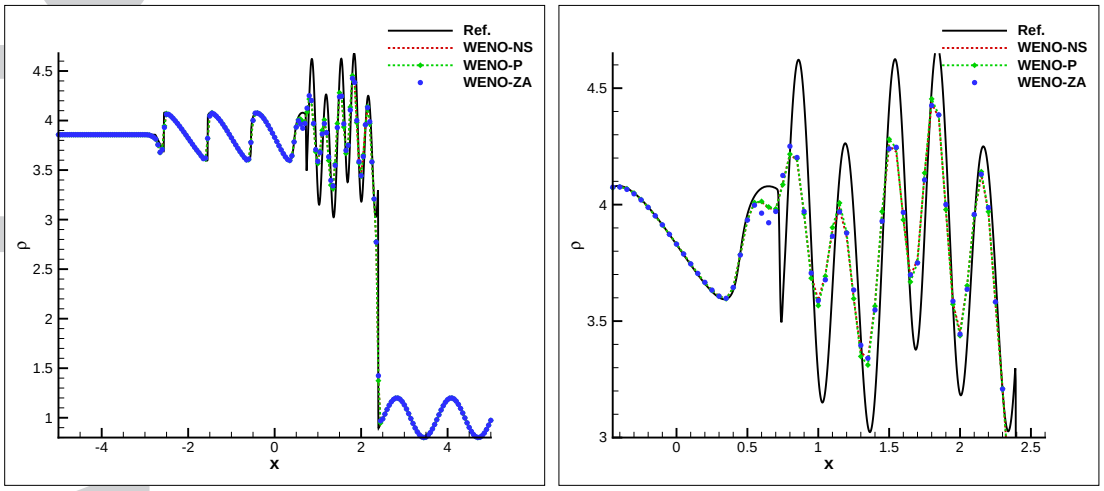

(a) (b)

Figure 14. Shu-Osher problem, $t = 1.8$, $N = 200$, using WENO-NS, WENO-P and WENO-ZA

*4.3.2. Case 6 * blast-waves interaction problem*

The second case is the blast-waves interaction problem[7] with the initial conditions,

$$(\rho, u, p) = \begin{cases} (1,\ 0,\ 1000), & 0 \le x < 0.1, \\ (1,\ 0,\ 0.01), & 0.1 \le x < 0.9, \\ (1,\ 0,\ 100), & 0.9 \le x \le 1. \end{cases} \tag{45}$$

The numerical results at $t = 0.038$ with $N = 300$ are presented in Fig.15. It can be seen, the WENO-ZA scheme obtains more accurate solution than the WENO-Z scheme. As already pointed out previously, in this case, due to the small value (0.01) of pressure, a small overshoot may generate negative pressure, hence, the WENO-Zη schemes as well as those schemes with unsuitable empirical parameters (WENO-NS, WENO-P) make the computation breakdown, and no results can be obtained. Hence, the WENO-Zη, WENO-NS and WENO-P schemes are no longer discussed and compared in the following two-dimensional problems.

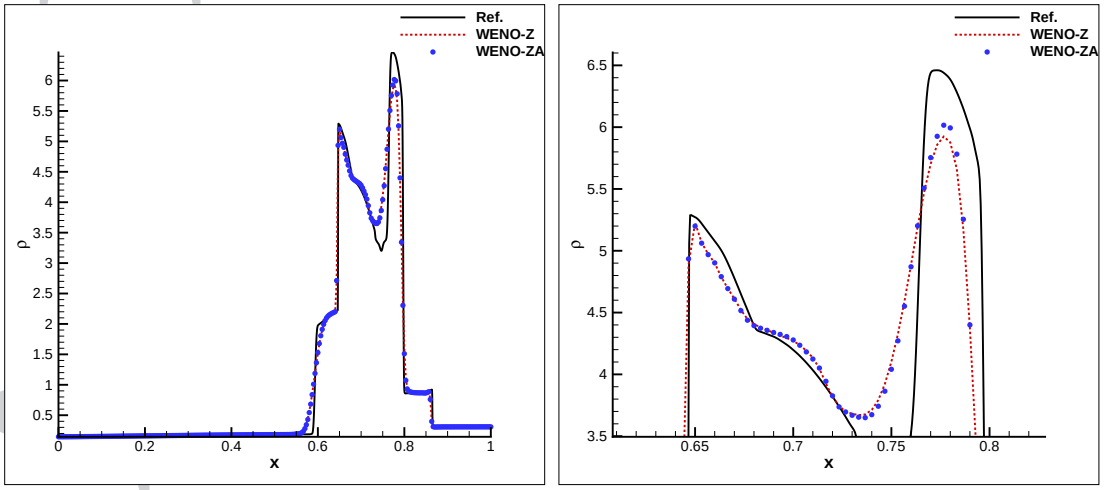

(a) (b)

Figure 15. Blast-waves interactive problem, $t = 0.038$, $N = 300$, using WENO-Z and WENO-ZA

4.4. Two-dimensional Euler problems

The governing equation is the two-dimensional Euler equations,

$$\frac{\partial U}{\partial t}+\frac{\partial F}{\partial x}+\frac{\partial G}{\partial y}=0, \tag{46}$$

where the conservative variables U, the inviscid flux vectors F and G are,

$$U=\begin{bmatrix}\rho\\ \rho u\\ \rho v\\ E\end{bmatrix},\ F=\begin{bmatrix}\rho u\\ \rho u^2+p\\ \rho uv\\ Eu+pu\end{bmatrix},\ G=\begin{bmatrix}\rho v\\ \rho uv\\ \rho v^2+p\\ Ev+pv\end{bmatrix}. \tag{47}$$

The energy is given by,

$$E=\frac{p}{\gamma-1}+\frac{\rho}{2}(u^2+v^2). \tag{48}$$

The Roe[18] flux-splitting method is used for the inviscid convective fluxes, and the time step is taken as follows,

$$\begin{aligned}\Delta t&=\sigma\frac{\Delta t_x\Delta t_y}{\Delta t_x+\Delta t_y},\\ \Delta t_x&=\frac{\Delta x}{max_{i,j}\left(|u_{i,j}|+c_{i,j}\right)},\\ \Delta t_y&=\frac{\Delta y}{max_{i,j}\left(|v_{i,j}|+c_{i,j}\right)}.\end{aligned} \tag{49}$$

4.4.1. Case 7 * periodic vortex propagation problem

This is a 2-D periodic vortex propagation problem[19, 20] used to assess the numerical dissipation of the finite-difference schemes. The vortex is described as a perturbation to the velocity $(u,\ v)$, temperature ($T=p/\rho$) and entropy ($S=p/\rho^\gamma$) of the mean flow $(\rho,\ u,\ v,\ p)=(1,\ 0.5,\ 0,\ 1)$,

$$\begin{cases}\hat{u}=-\dfrac{\epsilon e^{(1-r^2)/2}}{2\pi}\bar{y},\\ \hat{v}=\dfrac{\epsilon e^{(1-r^2)/2}}{2\pi}\bar{x},\\ \hat{T}=-\dfrac{(\gamma-1)\epsilon^2e^{(1-r^2)}}{8\gamma\pi^2},\\ \hat{S}=0,\end{cases} \tag{50}$$

where, $(\bar{x},\ \bar{y})=(x-5,\ y-5)$, $r^2=\bar{x}^2+\bar{y}^2$, and the vortex strength $\epsilon=0.5$. The computational domain is $[0,\ 10]\times[0,\ 10]$, and periodic boundary condition is used in both directions. The results at $t=1000$ with a grid of 50×50 are shown in Fig.16. Fig.17 gives the distributions of pressure and velocity v along x-axis at $y=5$ and the evolution of kinetic energy E_k, respectively. The kinetic energy is calculated by $E_k=\sum_{i,j=(1,1)}^{N,M}\rho_{i,j}(u_{i,j}^2+v_{i,j}^2)/2$. From these figures, it can be seen that, the WENO-ZA scheme performs as well as the upwind scheme (Up5), while the WENO-Z scheme shows larger dissipation.

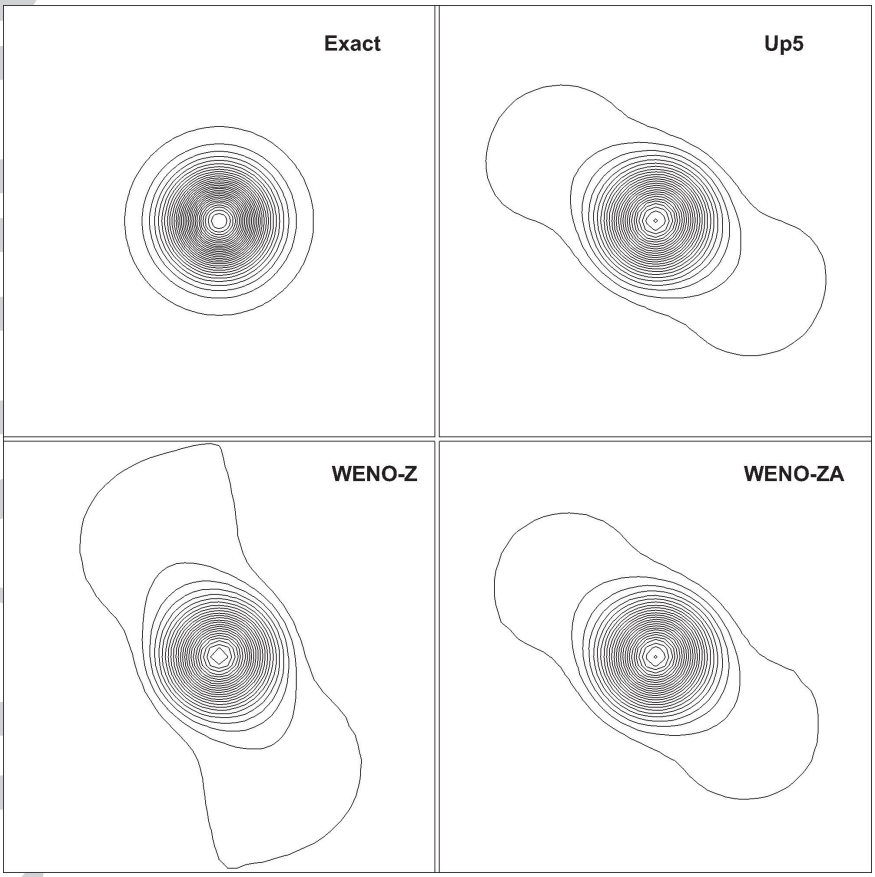

Figure 16. Pressure contours of the Vortex propagation problem: ranging from 0.9917 to 0.9999 with 30 equally separated levels

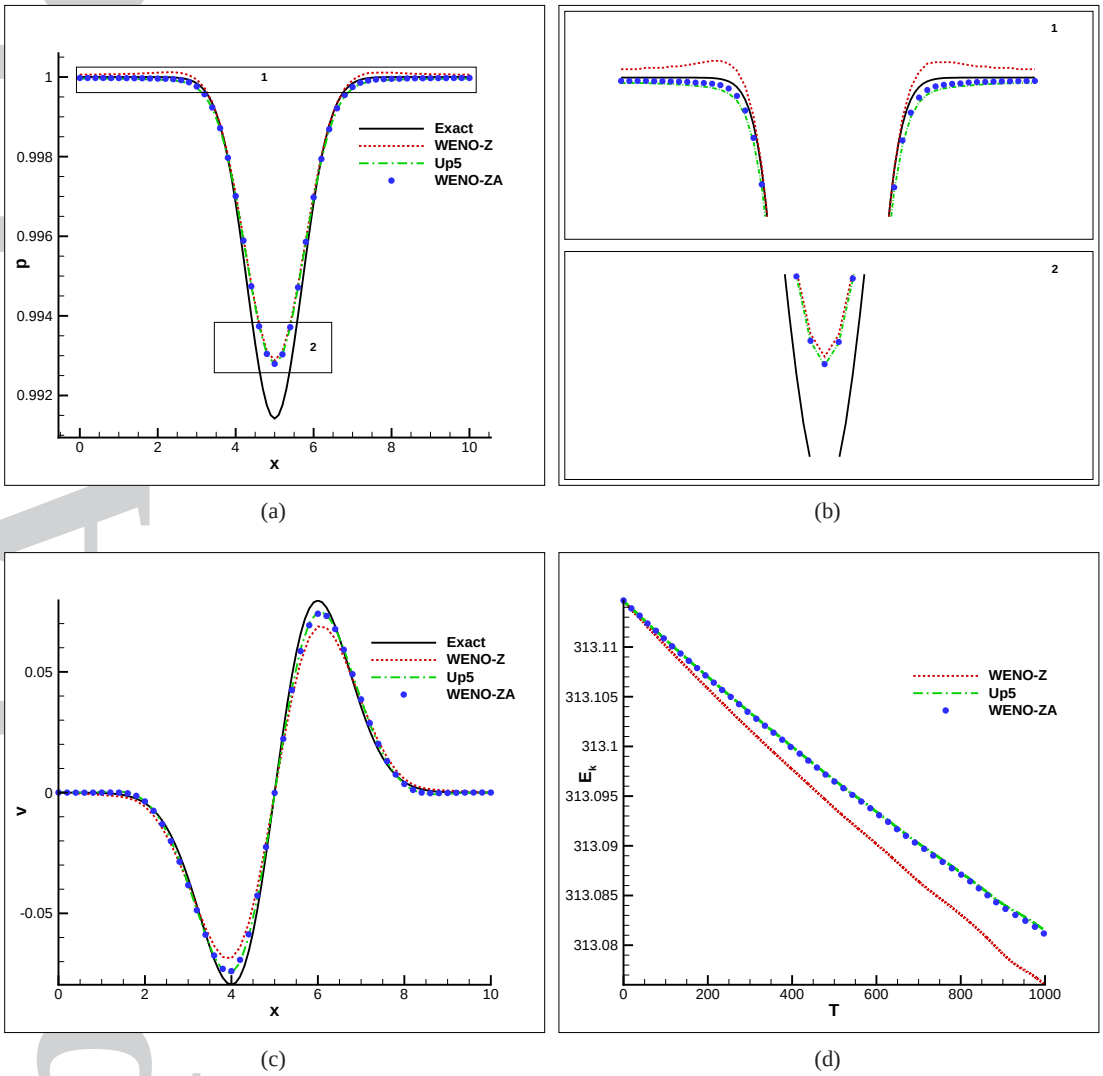

(a) (b)

(c) (d)

Figure 17. The distribution of pressure (a, b) and velocity v (c) along $y = 5$, and the evolution of kinetic energy E_k (d)

*4.4.2. Case 8 * Riemann problem*

This case is a two dimensional Riemann problem[9, 21] with the initial conditions,

$$(\rho, u, v, p) = \begin{cases} (1.5,\ 0,\ 0,\ 1.5), & 0.8 \le x \le 1, 0.8 \le y \le 1, \\ (0.5323,\ 1.206,\ 0,\ 0.3), & 0 \le x < 0.8, 0.8 \le y \le 1, \\ (0.138,\ 1.206,\ 1.206,\ 0.029), & 0 \le x < 0.8, 0 \le y < 0.8, \\ (0.5323,\ 0,\ 1.206,\ 0.3), & 0.8 \le x \le 1, 0 \le y < 0.8. \end{cases} \tag{51}$$

Two set meshes of 200×200 and 400×400 are used. The density contours at $t = 0.8$ are shown in Fig.18. It can be seen that both WENO-Z and WENO-ZA schemes can capture reflection shocks and contact discontinuities well. But the WENO-ZA scheme can resolve the roll-up of the Kelvin-Helmholtz instability with finer structures than the WENO-Z scheme.

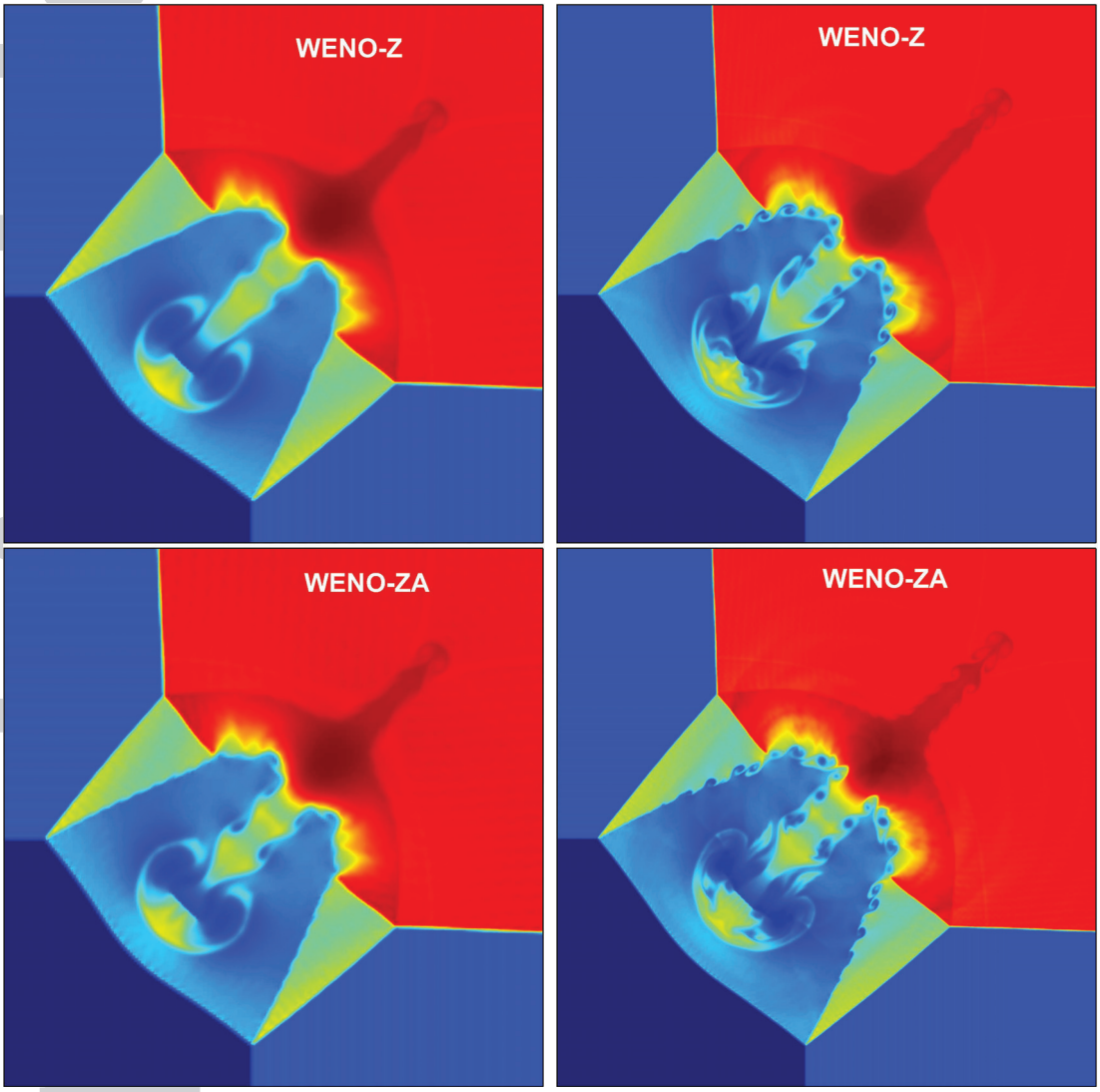

(a) The solutions with 200×200 (b) The solutions with 400×400

Figure 18. Density contours of Riemann problem

*4.4.3. Case 9 * Rayleigh-Taylor instability problem*

The two-dimensional Rayleigh-Taylor instability problem[22, 23] is often used to test the numerical dissipation of a high-order scheme. It describes the interface instability between fluids with different densities when acceleration is directed from the heavy fluid to the light one. The gravitational effect is introduced by adding ρ and ρv to the flux of the y-momentum and the energy equations, respectively. The initial distribution is,

$$(\rho, u, v, p) = \begin{cases} (2, 0, -0.025\alpha\cos(8\pi x), 2y + 1), & 0 \le y < 1/2, \\ (1, 0, -0.025\alpha\cos(8\pi x), y + 3/2), & 1/2 \le y \le 1, \end{cases} \tag{52}$$

and $\alpha = \sqrt{\gamma p/\rho}$ is the speed of sound with $\gamma = 5/3$. The computational domain is $[0, 0.25] \times [0, 1]$. The left and right boundaries are reflective boundary conditions, and the top and bottom boundaries are set as $(\rho, u, v, p) = (1, 0, 0, 2.5)$ and $(\rho, u, v, p) = (2, 0, 0, 1)$, respectively. The solution at $t = 1.95$ is solved with two meshes of 100×400 and 200×800. The density contours are plotted in Fig.19. Similar as observed in previous case, due to its less dissipation, the present scheme generates more complex instability structures than the WENO-Z scheme.

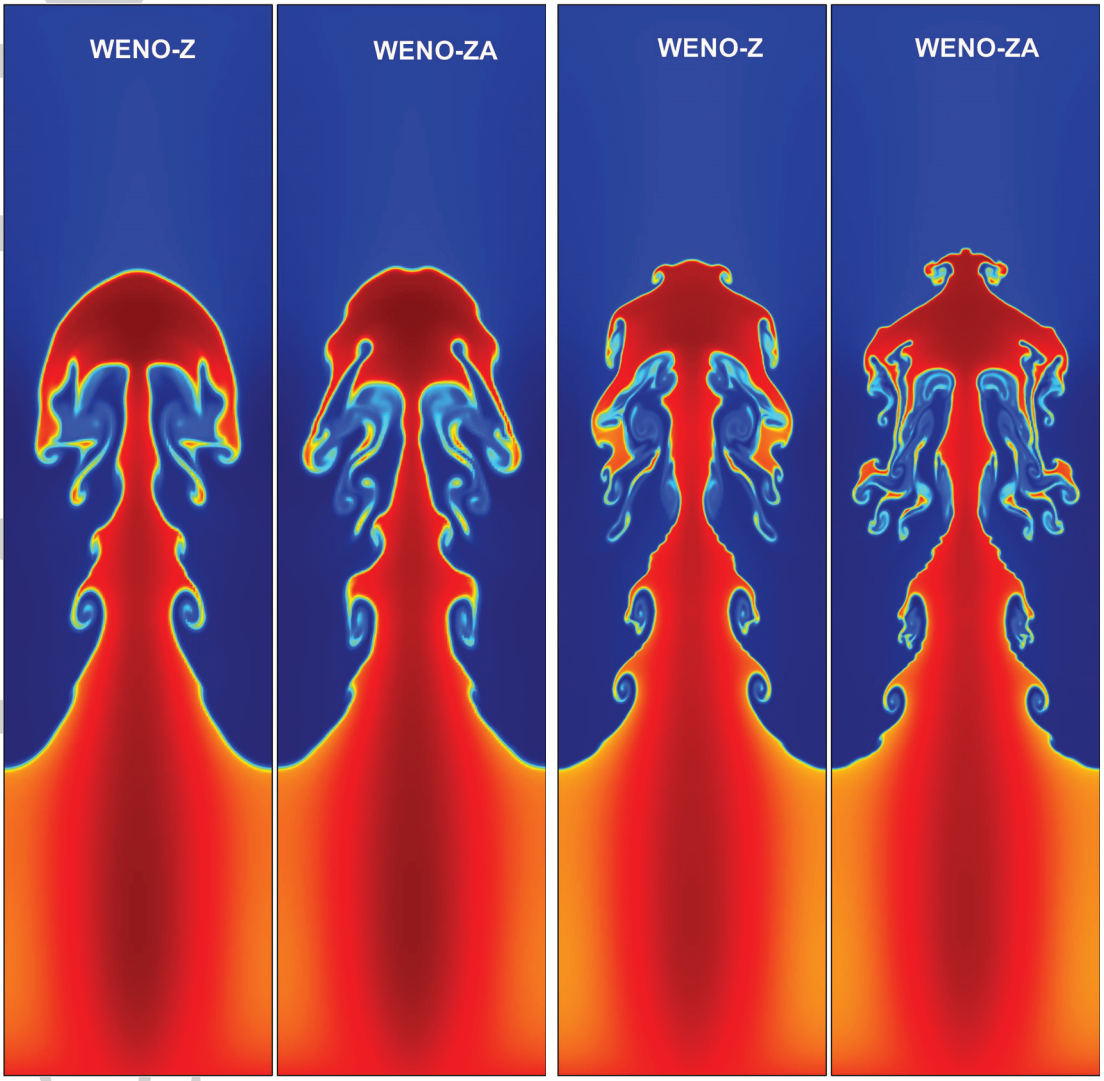

(a) The solutions with 100×400 (b) The solutions with 200×800

Figure 19. Density contours of Rayleigh-Taylor instability problem

5. CONCLUSION REMARKS

To improve the accuracy at critical points and keep low dissipation for the WENO-Z scheme, this paper proposes a sixth-order global smoothness indicator (GSI-6) and a function A about GSI-6 and the classical local smoothness indicators (IS_k). Using the multiplication of GSI-6 and the function to calculate the weights, the sufficient condition for fifth-order convergence in smooth regions including critical points is satisfied. Meanwhile, for a discontinuous global stencil, the weights assigned to those sub-stencils containing discontinuities are almost as large as those of the original WENO-Z scheme with power $q = 1$, hence the low dissipation is also maintained.

In fact, the multiplication of GSI-6 and the proposed function A can be regarded as an eighth-order global smoothness indicator (GSI-8). GSI-8 has the same dimension as the local smoothness indicators (IS_k), and there is no any problem-dependent parameter or grid spacing introduced. Hence, the proposed scheme with GSI-8 is more robust than most improved fifth-order WENO-Z schemes.

Furthermore, it is easy to extend the new idea to the third-order or higher-order WENO-Z-type schemes to improve their resolution.

ACKNOWLEDGEMENT

This research work was supported by the Grants NKRDPC 2016YFA0401200, NSAF U1530145, SCP No.TZ2016002 and NSFC 11272325.

REFERENCES

1. Shu CW. High order WENO and DG methods for time-dependent convection-dominated PDEs: A brief survey of several recent developments. *Journal of Computational Physics* 2016; **316**:598 – 613.
2. Liu XD, Osher S, Chan T. Weighted essentially non-oscillatory schemes. *Journal of Computational Physics* 1994; **115**:200 – 212.
3. Jiang GS, Shu CW. Efficient implementation of weighted ENO schemes. *Journal of Computational Physics* 1996; **126**:202 – 228.
4. Harten A. High resolution schemes for hyperbolic conservation laws. *Journal of Computational Physics* 1983; **49**:357 – 393.
5. Balsara DS, Shu CW. Monotonicity preserving weighted essentially non-oscillatory schemes with increasingly high order of accuracy. *Journal of Computational Physics* 2000; **160**:405 – 452.
6. Henrick AK, Aslam TD, Powers JM. Mapped weighted essentially non-oscillatory schemes: Achieving optimal order near critical points. *Journal of Computational Physics* 2005; **207**:542 – 567.
7. Borges R, Carmona M, Costa B, Don WS. An improved weighted essentially non-oscillatory scheme for hyperbolic conservation laws. *Journal of Computational Physics* 2008; **227**:3191 – 3211.
8. Marcos C, Bruno C, Sun DW. High order weighted essentially non-oscillatory WENO-Z schemes for hyperbolic conservation laws. *Journal of Computational Physics* 2011; **230**:1766–1792.
9. Ha Y, Kim CH, Lee YJ, Yoon J. An improved weighted essentially non-oscillatory scheme with a new smoothness indicator. *Journal of Computational Physics* 2013; **232**:68 – 86.
10. Kim CH, Ha Y, Yoon J. Modified non-linear weights for fifth-order weighted essentially non-oscillatory schemes. *Journal of Scientific Computing* 2016; **67**:299 – 323.
11. Fan P, Shen YQ, Tian BL, Yang C. A new smoothness indicator for improving the weighted essentially non-oscillatory scheme. *Journal of Computational Physics* 2014; **269**:329 – 354.
12. Hu X, Wang Q, Adams N. An adaptive central-upwind weighted essentially non-oscillatory scheme. *Journal of Computational Physics* 2010; **229**:8952 – 8965.
13. Acker F, de R Borges RB, Costa B. An improved WENO-Z scheme. *Journal of Computational Physics* 2016; **313**:726 – 753.
14. Shen YQ, Zha GC. A robust seventh-order WENO scheme and its application. *AIAA Paper 2008-0757* 2008; .
15. Pirozzoli S. On the spectral properties of shock-capturing schemes. *Journal of Computational Physics* 2006; **219**:489–497.
16. Shu CW, Osher S. Efficient implementation of essentially non-oscillatory shock-capturing schemes. *Journal of Computational Physics* 1988; **77**:439 – 471.
17. Shu CW. Essentially non-oscillatory and weighted essentially non-oscillatory schemes for hyperbolic conservation laws. *ICASE Report 97-65* 1997; .
18. Roe PL. Approximate Riemann solvers, parameter vectors, and difference schemes. *Journal of computational physics* 1981; **43**:357–372.
19. Sun YZ, Wang Z. Evaluation of discontinuous galerkin and spectral volume methods for scalar and system conservation laws on unstructured grids. *International Journal for Numerical Methods in Fluids* 2004; **45**:819 – 838.
20. Davoudzadeh F, McDonald H, Thopson B. Accuracy evaluation of unsteady CFD numerical schemes by vortex preservation. *Computational & Fluids* 1995; **24**:883 – 895.
21. Balsara DS. Multidimensional HLLE Riemann solver: Application to Euler and magnetohydrodynamic flows. *Journal of Fluid Mechanics* 2010; **229**:1970 – 1993.
22. Shi J, Zhang YT, Shu CW. Resolution of high order WENO schemes for complicated flow structures. *Journal of Computational Physics* 2003; **186**:690 – 696.
23. Yong YN, Tufo H, dubey A, Rosner R. On the miscible Rayleigh-Taylor instability: two and three dimensions. *Journal of Fluid Mechanics* 2001; **447**:337 – 408.